Coarse Nb_3Sn Grain Formation and Phase Evolution During the Reaction of a High Sn Content Internal Tin Strand

C. Scheuerlein, M. Di Michiel, G. Arnau, R. Flükiger, F. Buta, I. Pong, L. Oberli, and L. Bottura

Abstract—The formation of coarse Nb_3Sn grains in Internal Tin (IT) strands has been studied at the example of a prototype strand with high Sn content. Metallographic examination revealed that the comparatively low critical current density (J_c) of this strand is partly due to the formation of a significant fraction of coarse grained Nb_3Sn at the periphery of the individual filaments within the subelements. The phase evolution during the reaction heat treatment has been determined *in situ* by high energy synchrotron X-ray diffraction as well as *ex situ* by Energy Dispersive X-ray Spectroscopy in a Scanning Electron Microscope (SEM) in order to identify the conditions under which the coarse grains form. Similar to what is observed in the tubular type strands, Nb_3Sn coarse grain formation occurs in the filament areas that had first been transformed into $NbSn_2$ and Nb_6Sn_5, prior to Nb_3Sn formation, and it accounts for an estimated J_c reduction of roughly 20%. The amount of Cu–Nb–Sn and $NbSn_2$ that is formed during the heat treatment can be reduced by increasing the temperature ramp rate, while the amount of Nb_6Sn_5 formed appears to be hardly influenced by the different heat treatments that have been tested.

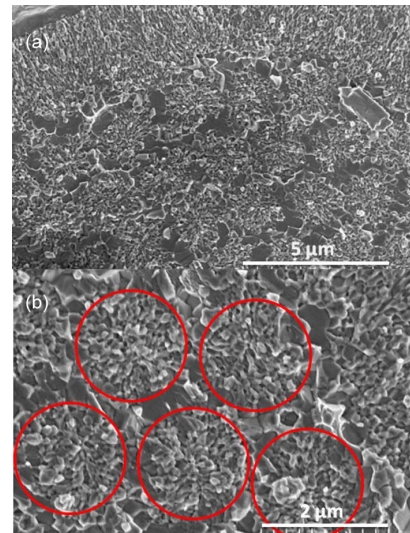*Index Terms*—Nb_3Sn, superconducting wires and filaments.

Fig. 1. (a) SEM image of a fractured sample of the B1-63468 strand reacted 50 h at 660 °C. The coarse grains are present around the location of the original Nb filaments, as shown by the red circles in (b).

I. INTRODUCTION

IT IS well known that during the reaction heat treatment of Nb_3Sn strands with high Sn contents, e.g. Internal Tin (IT) or Powder-in-Tube (PIT) strands, several intermediate phases are formed, which decompose again before the final A15 phase is formed. The succession of phases can have a strong influence on the Nb_3Sn grain size and microchemistry in the fully reacted state. This is best observed in the tubular strand types (Powder-in-Tube (PIT) [1] and Tube Type [2]), where an important fraction of Nb_3Sn is present in the form of coarse grains. In PIT strands typically 25% of Nb_3Sn consist of coarse grains [3] and similar amounts of coarse grain Nb_3Sn are observed in Tube Type strands [4]. In restack rod processed (RRP) IT

strands, coarse Nb_3Sn grains are observed too, but their amount with respect to the entire Nb_3Sn volume is comparatively small [5].

In this article we describe the phase sequence during the reaction heat treatment of a prototype IT strand with high Sn content and its influence on the formation of coarse Nb_3Sn grains. This prototype strand (in the following referred to as B1-63468) has been produced in the frame of the Next European Dipole conductor development program and does not contain Ta or Ti additions. Its non-Cu critical current density (J_c) remained below 1500 A/mm^2@4.2 K at 12 T. For comparison, this value is less than half of the highest J_c values obtained routinely for long lengths of Ta or Ti alloyed Internal Sn strands of the RRP design [6].

As revealed by metallographic analysis of fractured samples after reaction of 50 h at 660 °C (see Fig 1), one reason for the comparatively low J_c of the B1-63468 sample is a comparatively large fraction of coarse grained Nb_3Sn that is formed around each filament. Under the assumption of a negligible contribution of coarse Nb_3Sn grains to the current transport, their presence is thought to be partly responsible for the unexpectedly low J_c values of the prototype strand.

The phase formation sequence was determined by high energy synchrotron X-ray diffraction measurements performed *in situ* during reaction. The influence of different ramp rates and
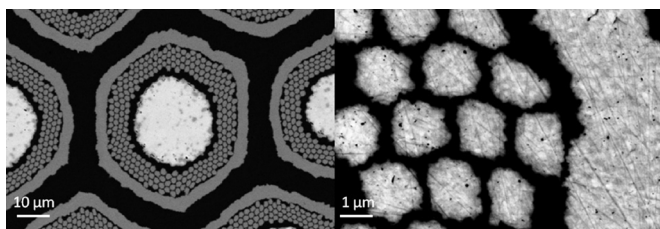
Fig. 2. Cross section of an unreacted B1-63468 sub-element.

long lasting low temperature plateaus on the amount of the different intermetallic phases formed is described. Phase identification with spatial resolution was performed by means of Energy Dispersive X-ray Spectroscopy (EDS) measurements in a Scanning Electron Microscope (SEM).

II. EXPERIMENTAL

A. Binary B1-63468 Nb_3Sn Strand

A cross section of the prototype B1-63468 strand with 246 subelements is shown in Fig. 2. The strand has a nominal diameter of 1.25 mm and a Cu/non-Cu ratio of 1.08. The minimal diameter of the hexagonal subelements is about 53 μm. Each subelement (nominal composition Nb-53.6, Sn-25.1, Cu-21.3 vol.%) consists of 246 filaments of about 1.8 μm diameter and a diffusion barrier with an approximate thickness of 3.6 μm. The nominal Nb/Sn atomic % ratio is 3.2 (including the Nb barrier). The filaments and the barrier are made of pure Nb. The nominal Cu to Nb local area ratio is 0.3.

B. In Situ Synchrotron X-ray Diffraction

Synchrotron X-ray diffraction measurements were carried out at the ID15B high energy scattering beamline of the European Synchrotron Radiation Facility (ESRF), using a 86.926 keV monochromatic X-ray beam. The high transmission of the high energy X-rays through the highly absorbing metallic samples enables nondestructive diffraction measurements. Debye–Scherrer diffraction patterns were acquired with a Trixell Pixium 4700 detector, with a sample to detector distance of 1004.3 mm. Heating was performed in a dedicated X-ray transparent furnace built at ID15, the sample temperature during diffraction being controlled to $\pm10\,^\circ$C.

C. SEM and EDS

Strand cross sections were observed with a SEM Leo 430 using a 20-keV electron beam and a solid state diode detector for recording backscattered-electron (BSE) images. The compositional contrast given by the BSE images (regions of increasing atomic number appearing increasingly brighter) allowed the visualization of the constituents of the strand microstructure to a resolution better than 0.1 μm. An EDS system Oxford Isis 300 with a Si(Li) detector coupled to the SEM was used in the standardless mode for the quantitative elemental analysis. For the constituents of small size (of the order of the micrometer), the largest regions were targeted to overcome the relatively poor lateral resolution of the EDS point analysis (at least one order of magnitude lower than BSE imaging).
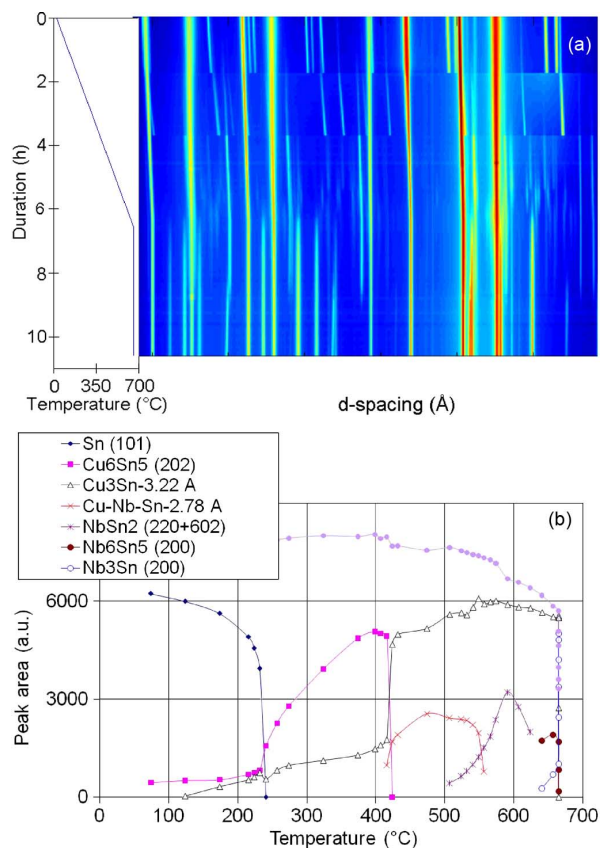

Fig. 3. (a) Variation of the diffraction patterns of the B1-63468 strand during a temperature ramp of 100 $^\circ$C/h. The temperature resolution is 8 $^\circ$C. The evolution of selected peak areas is shown in (b). Peak areas have been arbitrarily scaled in order to fit into the plot.

III. RESULTS

A. In Situ Synchrotron X-ray Diffraction up to 665 $^\circ$C

Diffraction measurements have been performed *in situ* during different temperature ramps and at a final plateau at 665 $^\circ$C. In order to study the influence of the ramp rate, the amounts of the different phases formed during a very fast temperature ramp of 600 $^\circ$C/h have been compared with those formed during a 100°C/h ramp. The influence of long plateaus at lower temperature has been studied during a 100 $^\circ$C/h ramp applied to a sample that had been heat treated in for 314 h at 200 $^\circ$C and 50 h at 400°C, prior to the diffraction measurements.

The sequence of diffractograms acquired during the reaction of the B1-63468 strand with a ramp rate of 100 $^\circ$C/h and a subsequent isothermal heat treatment at 665 $^\circ$C is presented in the color intensity diagram shown in Fig. 3(a). The corresponding evolution of selected diffraction peak areas is shown in Fig. 3(b).

Before the onset of Nb_3Sn formation, four intermetallic phases have been identified by comparison with published reference diffraction pattern: Cu_6Sn_5, Cu_3Sn, $NbSn_2$, and Nb_6Sn_5. In addition the diffraction pattern of a presumed Cu–Nb–Sn ternary phase was detected. All these phases have previously been detected during the reaction of Nb_3Sn strands of the PIT [7], Tube Type [8] and RRP [5] design. The temperature regions where the different intermetallic phases are
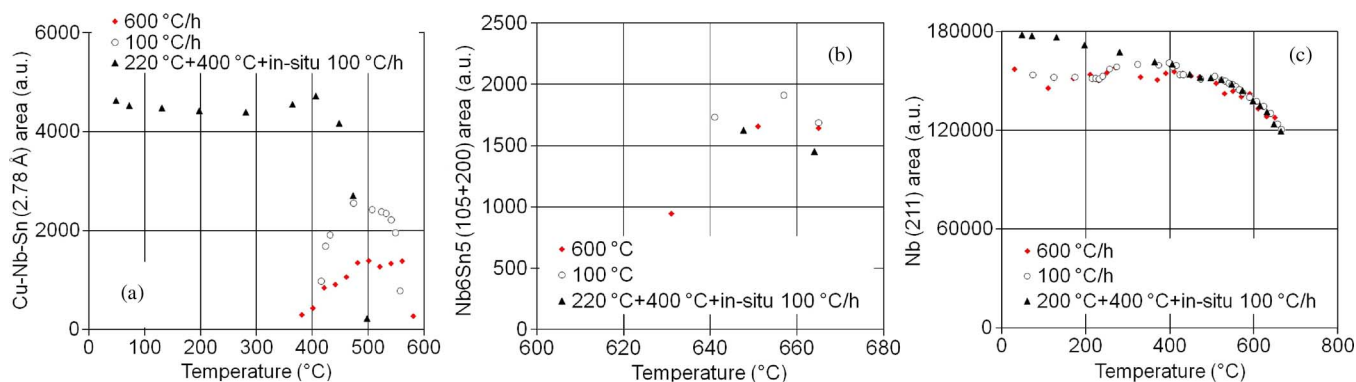
Fig. 4. (a) Cu–Nb–Sn peak with $d = 2.78$ Å, (b) Nb_6Sn_5 (105)+(200), and (c) Nb (211) peak area evolution during heat treatment of the B1-63468 strand with different ramp rates.

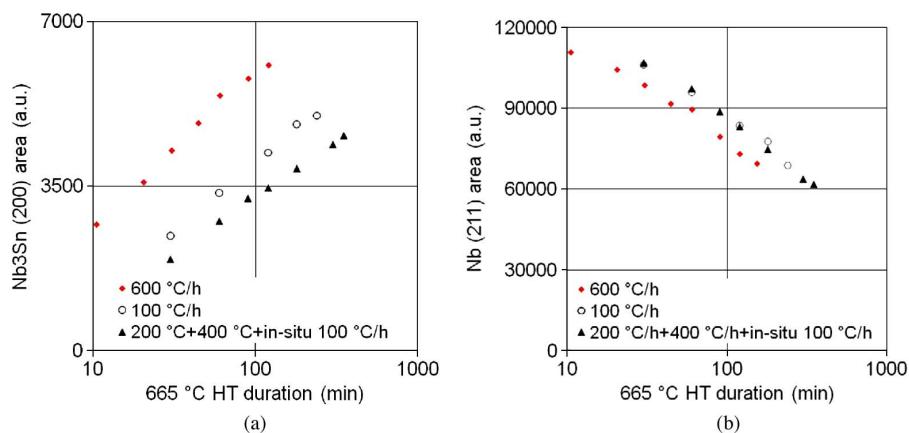Fig. 5. Evolution of the Nb_3Sn (200) and Nb (211) peak area of the B1-63468 strand during isothermal heat treatment at 665 °C subsequent to heating with different ramp rates.

detected are similar to those determined by diffraction measurements for the other high Sn Nb_3Sn strands [8].

The evolution of selected Cu–Nb–Sn, Nb_6Sn_5 and Nb peak areas during the three different heating ramps (600 °C/h, 100°C/h, and 100 °C/h subsequent to 314 h at 200 °C and 50 h at 400 °C) is shown in Fig. 4. The ramp rate has a significant influence on the maximum amount of the Cu_6Sn_5, Cu–Nb–Sn and $NbSn_2$ formed (Cu_6Sn_5, and $NbSn_2$ results are not shown in Fig. 4). With the faster temperature ramp, less of these phases are formed. $NbSn_2$ formation can be largely avoided and the amount of Cu–Nb–Sn strongly decreased when heating with 600 C/h. Assuming that the Nb that is dissolved in the ternary Cu–Nb–Sn phase is not transferred into fine grained Nb_3Sn later on, it can be concluded that long lasting low temperature plateaus in the temperature range where the ternary Cu–Nb–Sn phase forms can be counterproductive for improving J_c of the fully reacted strand.

The Nb_6Sn_5 peaks are comparatively small, thus rendering Nb_6Sn_5 peak area measurements difficult. Nevertheless it can be concluded from the Nb_6Sn_5 peak area measurements shown in Fig. 4(b) that the amount of Nb_6Sn_5 is not strongly influenced by the ramp rate.

Above 400 °C, the evolution of the Nb (211) peak area as a function of temperature is within the experimental error identical for all three temperature ramp rates [see Fig. 4(c)]. The differences in the Nb (211) areas measured at lower temperatures

may be caused by a different spatial distribution of the strongly absorbing Sn in the subelements of the strand heated for 314 h at 200 °C+50 h at 400 °C and in the strands without prior treatment. Variations of the texturing of the strongly cold drawn Nb precursor could be another explanation. However, to our knowledge Nb recrystallization at temperatures below 400 °C has not been reported.

Assuming that above 415 °C, the Cu_6Sn_5 decomposition temperature, the Nb (211) peak area is proportional to the amount of Nb present in the strand, it can be estimated that in the B1-63469 strand roughly 20% of Nb is transformed into Cu–Nb–Sn, $NbSn_2$ and finally Nb_6Sn_5, and this part of Nb is lost for the formation of fine grained Nb_3Sn.

The Nb_3Sn (200) peak area evolution during the different heat treatments is compared in Fig. 5(a). The results may indicate that the growth of Nb_3Sn subsequent to a 600 °C/h ramp is somewhat faster than the growth following the slower temperature ramps. The onset temperature at which the Nb_3Sn diffraction pattern is detected when heating with a ramp rate of 100°C/h is about 650 °C.

B. SEM/EDS Results

Phase analysis with micrometer spatial resolution has been performed on polished strand cross sections, as a complement to the diffraction results. Individual heat treatments of 10 h at 380 °C, 440 °C, 490 °C, and 590 °C have been achieved under
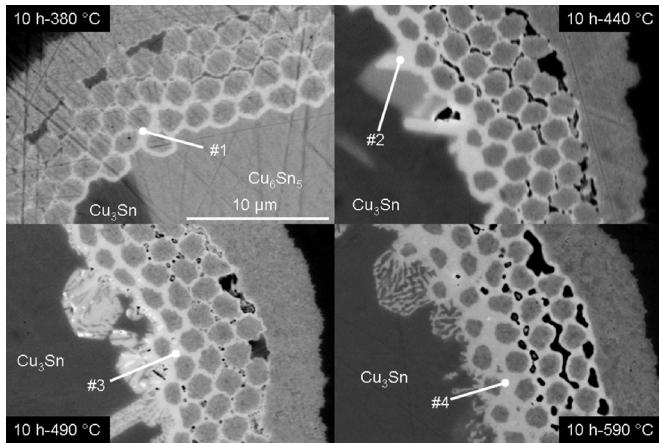
Fig. 6.   BE-SEM image of B1-63468 strand cross sections after 10 h at 380 °C, 440 °C, 490 °C, and 590 °C.

TABLE I
ELEMENTAL COMPOSITION AS DETERMINED BY EDS AND IDENTIFIED PHASES

	Composition in at.% *	Main phase identified
#1	Cu-10.4, Nb-39.0, Sn-50.6	Presumed ternary Cu-Nb-Sn
#2	Cu-18.1, Nb-17.1, Sn-64.8	Presumed ternary Cu-Nb-Sn
#3	Cu-3.7, Nb-38.5, Sn-57.8	$NbSn_2$ + Cu
#4	Cu-5.7, Nb-50.2, Sn-44.1	Nb_6Sn_5 + Cu

*Semiquantitative EDS results of interfilament material overestimate the Nb content due to the proximity of the Nb filaments.

vacuum, each with a ramp rate of 60 °C/h. BSE images of the respective cross sections are shown in Fig. 6.

The elemental compositions determined by EDS in the different cross sections are summarized in Table I. The EDS results overestimate the amount of Nb, due to the proximity of the unreacted Nb filaments. Nevertheless, in spite of the limited spatial resolution of EDS measurements in the SEM and the comparatively small size of the phases of interest, it is possible to distinguish between the presumed Cu–Nb–Sn ternary phase, $NbSn_2$ and Nb_6Sn_5.

After 10 h at 380 °C the matrix is partly in the form of Cu_6Sn_5 and Cu_3Sn and the presumed Cu–Nb–Sn ternary phase is detected around the individual filaments. During the 10 h–440 °C treatment most Cu_6Sn_5 has been transformed into Cu_3Sn, but a small amount of Cu_6Sn_5 is still detected. Since the Cu_6Sn_5 decomposition temperature is 415 °C, this indicates that liquid Sn was present at the end of the 10 h–440°C treatment, which was retransformed into Cu_6Sn_5 upon cool down [7]. EDS analysis indicates that the material with relatively high atomic number around the filaments is still the presumed Cu–Nb–Sn ternary phase. After 10 h at 490 °C $NbSn_2$ is detected at the circumference of the filaments closest to the Sn source, and after the 10 h at 590 °C the $NbSn_2$ is transformed into Nb_6Sn_5.

IV. DISCUSSION AND CONCLUSION

The problem of coarse Nb_3Sn grain formation in the IT strand studied here, which also occurs in the PIT and Tube Type

strands, and to a much smaller extent in the OI-ST RRP strand [5], is related to the high Sn content needed to reach high J_c values. To our best knowledge, in low hysteresis loss IT strands with a much higher Cu/Sn ratio inside the subelements, the formation of coarse Nb_3Sn grains has not been reported.

From metallographic examination (see Fig. 6) it can be concluded that, like in the tubular strands, in the B1-63468 strand the Nb_3Sn formed from the orthorhombic Nb_6Sn_5 has much larger grains than the Nb_3Sn formed by a diffusion process from the cubic Nb, without intermediate Nb_6Sn_5 formation. Thus, in order to reduce the amount of coarse Nb_3Sn in the fully reacted strand, it is necessary to reduce the amount of Nb_6Sn_5 that is formed during the reaction treatment.

The temperature ramp rate influences the amount of Cu–Nb–Sn and $NbSn_2$, but does not have a strong influence on the amount of Nb_6Sn_5. Therefore, it is concluded that the formation of coarse Nb_3Sn grains can not be avoided by employing very fast ramp rates. Even if they did lead to a reduction in the quantity of large grains, very fast ramp rates like the 600 °C/h studied here can not be easily applied to magnet coils. However, excessively long temperature ramps can be counterproductive and can cause a degradation of J_c due to the dissolution of Nb in the form of the presumed Cu–Nb–Sn ternary phase. Long durations spent in the approximate temperature interval of 350–550 °C, where the Cu–Nb–Sn phase is observed, should be avoided. A detrimental effect of isothermal plateaus on the microchemical homogeneity has also been observed for an IT strand with comparatively high Cu/Sn ratio [9].

Several attempts have been made to reduce the amount of coarse grained Nb_3Sn in PIT strands by varying the subelement layout and composition (use of different precursors, alloying, etc.) [10], but in today's state-of-the-art PIT strands a relatively large amount of coarse Nb_3Sn grains is still present. In contrast, in IT strands of the RRP design it is possible to strongly limit the Nb_6Sn_5 growth and, as a result, only a very small amount of coarse Nb_3Sn is formed [8].

The formation of Nb_6Sn_5 and coarse grained Nb_3Sn seems to be linked to the Sn content around the filaments in the relevant temperature range, and possibly to the presence of liquid Sn at the filament periphery. As can be seen in Fig. 6, the closer the Nb precursor to the Sn source, the more Nb_6Sn_5 (and coarse Nb_3Sn) is formed.

Unlike in the tubular strands, the diffusion path lengths and spacing in IT strands can be varied by varying the filament size and the local Cu to Nb area ratio (LAR). As compared to high J_c IT strands [11], the B1-63468 LAR of 0.3 is relatively high. Therefore, for high Sn strands it is assumed that reducing the LAR is beneficial in order to reduce the amount of coarse Nb_3Sn volume. As outlined above, if formation of coarse Nb_3Sn grains could be avoided this could cause a J_c increase of roughly 20% in the B1-63468 strand.

In this article only the formation of coarse Nb_3Sn grains is addressed as one reason for the comparatively low J_c of the B1-63468 strand. Other possible reasons for the comparatively low J_c of this strand include the absence of any alloying elements [12] and the Sn distribution within the A15 phase. Both, the microchemical strand homogeneity and the high average Sn content are important parameters that can strongly influence the

critical temperature (T_c), the critical field (B_{c2}) and, as a result the critical current density [13].

REFERENCES

[1] H. Veringa, E. M. Hornsveld, and P. Hoogendam, *Adv. Cryo. Eng.*, vol. 30, pp. 813–821, 1984.

[2] E. Gregory, X. Peng, M. Tomsic, M. D. Sumption, and A. Ghosh, "Nb_3Sn superconductors made by an economical tubular process," *IEEE Trans. Appl. Supercond.*, vol. 19, no. 3, pt. 3, pp. 2602–2605, 2009.

[3] M. Fischer, "Investigation of the relationships between superconducting properties and reaction conditions in powder-in-tube Nb_3Sn conductors," M.Sc. thesis, University of Wisconsin, Madison, WI, 2002.

[4] V. R. Nazareth, M. D. Sumption, X. Peng, E. Gregory, M. J. Tomsic, and E. W. Collings, "Characterization of the A15 layer growth and microstructure for varying heat treatments in Nb_3Sn tube type composites," *IEEE Trans. Appl. Supercond.*, vol. 18, no. 2, pp. 1005–1009, 2008.

[5] C. Scheuerlein, M. Di Michiel, G. Arnau, and F. Buta, "Phase transformations during the reaction heat treatment of internal tin Nb_3Sn strands with high Sn content," *IEEE Trans. Appl. Supercond.*, vol. 18, no. 4, pp. 1754–1760, 2008.

[6] J. A. Parrell, Y. Zhang, M. B. Field, and S. Hong, "Development of internal tin Nb_3Sn conductor for fusion and particle accelerator applications," *IEEE Trans. Appl. Supercond.*, vol. 17, no. 2, pp. 2560–2563, 2007.

[7] M. Di Michiel and C. Scheuerlein, "Phase transformations during the reaction heat treatment of powder-in-tube Nb_3Sn superconductors," *Supercond. Sci. Technol.*, vol. 20, pp. L55–L58, 2007.

[8] C. Scheuerlein, M. Di Michiel, L. Thilly, F. Buta, X. Peng, E. Gregory, J. A. Parrell, I. Pong, B. Bordini, and M. Cantoni, "Phase transformations during the reaction heat treatment of Nb_3Sn superconductors," *J. Phys.: Conf. Ser.*, vol. 234, p. 022032, 2010.

[9] C. Scheuerlein, M. Di Michiel, and A. Haibel, "On the formation of voids in Nb_3Sn superconductors," *Appl. Phys. Lett.*, vol. 90, p. 132510, 2007.

[10] A. Godeke, A. den Ouden, A. Nijhuis, and H. H. J. ten Kate, " State of the art powder-in-tube niobium-tin superconductors," *Cryogenics*, vol. 48, pp. 308–316, 2008.

[11] M. Field, J. Parrell, Y. Zhang, and S. Hong, "Critical current density in Nb_3Sn superconducting wire," U.S. Patent US 7368021 B2, May 2008.

[12] R. Flükiger, D. Uglietti, C. Senatore, and F. Buta, "Microstructure, composition and critical current density of superconducting Nb_3Sn wires ," *Cryogenics*, vol. 48, pp. 293–307, 2008.

[13] P. J. Lee and D. C. Larbalestier, "Microstructural factors important for the development of high critical current density Nb_3Sn strand," *Cryogenics*, vol. 48, pp. 283–292, 2008.